International Journal of Thermal Sciences 49 (2010) 1209–1226

Contents lists available at ScienceDirect

International Journal of Thermal Sciences

journal homepage: www.elsevier.com/locate/ijts

Large eddy simulations of wall heat transfer and coherent structures in mixed convection over a wavy wall

Simon Kuhn [a,1], Saša Kenjereš [b,*], Philipp Rudolf von Rohr [a]

[a] Transport Processes and Reactions Laboratory, Institute of Process Engineering, ETH Zurich, Sonneggstrasse 3, 8092 Zurich, Switzerland
[b] Department of Multi-Scale Physics, Faculty of Applied Sciences and J. M. Burgerscentre for Fluid Dynamics, Prins Bernhardlaan 6, 2628 BW Delft, The Netherlands

ARTICLE INFO

Article history:
Received 3 June 2009
Received in revised form
17 December 2009
Accepted 15 January 2010
Available online 19 February 2010

Keywords:
Large eddy simulation
Mixed convection
Wavy wall
Vortical flow structures
Wall heat transfer

ABSTRACT

In this numerical study the mixed convective flow of water over a heated wavy surface over a range of Reynolds and Richardson numbers, including transitional and turbulent flow regimes ($20 \leq Re \leq 2000$ and $0.5 \leq Ri \leq 5000$) is investigated. A dynamic Large Eddy Simulation (LES) approach is applied where the thermal buoyancy effects are represented by the Boussinesq approximation. The LES results show good agreement with available measurements including first and second order statistics of velocity and thermal fields. We focus our investigation on the thermal buoyancy effects on the wall heat transfer and the spatial reorganisation of the vortical flow structures. In order to characterise the reorganisation of the mean flow features, the vortical coherent structures are identified and extracted according to the swirling strength criteria. Interesting reorganisation of flow structures takes place between $Re = 20$ and $Re = 200$ where the initially spanwise oriented large coherent structures start to be streamwise oriented. With further increase of Re, these large structures disappear from the central part of the simulated domain and reappear in the proximity of the horizontal wavy wall for $Re \geq 1000$. The imprints of this flow reorganisation are clearly visible in the distributions of the local heat transfer coefficient (Nusselt number) along the horizontal wavy wall. The integral heat transfer for the wavy wall configuration is significantly enhanced ($\approx$2.5 times) for $Re = 1000, 2000$ in comparison with the standard flat horizontal wall configuration.

1. Introduction

Mixed convective flows are present in technical applications, such as heat transfer devices, and in geophysical flow situations such as transport processes in plant canopies, Banna et al. [1]. These mixed convective flows are often bound by complex wall geometries, e.g. undulations in heat exchangers to enhance transport processes (e.g. Rush et al. [2], Dellil et al. [3]). In the present study we numerically investigate the mixed convective channel flow between a flat top wall and a heated wavy bottom wall at Richardson numbers ranging from $Ri = Gr/Re^2 = 0.5$ to 5000. The Grashof number Gr is defined as [4]

$$Gr = \frac{gH^4\dot{q}\beta}{\nu^2\lambda}, \tag{1}$$

where H denotes the height of the channel, $\dot{q}$ is the heat flux applied on the bottom wall, and β is the volumetric thermal expansion coefficient. The effect of buoyancy induced fluid motions together with the influence of the wavy bounding surface on the mean flow and the wall heat transfer is addressed. We compare our numerical predictions with experimental results of a wavy channel flow facility with the same geometrical configuration and boundary conditions.

Previous experimental studies of mixed convective channel flows focused mainly on horizontal parallel plate configurations. Osborne and Incropera [5,6], experimentally investigated laminar, transitional, and turbulent mixed convection heat transfer for a horizontal parallel plate water channel. Their studies covered Reynolds numbers in the range of $65 \leq Re \leq 6500$, and Grashof numbers between $4.2 \times 10^5 \leq Gr \leq 2.8 \times 10^8$. They found an increase in heat transfer due to buoyancy effects by a factor of 6 in the laminar flow regime. This heat transfer enhancement was significantly reduced for higher values of Reynolds numbers where a factor of 1.3 was obtained. Maughan and Incropera [7] analysed the regions of heat transfer enhancement for laminar mixed convection for the same flow configuration with $2 \times 10^4 \leq Gr \leq 8 \times 10^5$ at

* Corresponding author.
E-mail address: S.Kenjeres@tudelft.nl (S. Kenjereš).
[1] Present address: Massachusetts Institute of Technology, Cambridge, USA.

1290-0729/$ – see front matter © 2010 Elsevier Masson SAS. All rights reserved.
doi:10.1016/j.ijthermalsci.2010.01.017

Nomenclature

Upper case Roman

A	anisotropy flatness parameter
C_s	Smagorinsky constant
Gr	Grashof number for channel flow, $gH^4\dot{q}\beta/(\nu^2\lambda)$
H	full channel height, m
Nu	Nusselt number
Pr	Prandtl number
Pr_t	Turbulent Prandtl number
Ra	Rayleigh number for channel flow, Ra = GrPr
Re	Reynolds number for channel flow, $U_B H/\nu$
Ri	Richardson number, $\mathrm{Ri} = \mathrm{Gr}/\mathrm{Re}^2$
$\overline{S_{ij}}$	rate of strain tensor, 1/s
$\overline{T}$	temperature, K
U_B	bulk velocity (channel flow), m/s
U_m	mixed velocity, m/s

Lower case Roman

a	half-amplitude of the wave profile, m
a_{ij}	anisotropy tensor
g	acceleration due to gravity, $\mathrm{m/s}^2$
$\dot{q}$	heat flux, $\mathrm{W/m}^2$
$\overline{u}, \overline{v}, \overline{w}$	resolved velocity components, m/s
u_τ	friction velocity, m/s
x, y, z	Cartesian coordinates, m
x_R	reattachment point, m
x_S	separation point, m
y_w	profile of the wavy bottom wall, m

Upper Greek symbols

Δ	LES filter width, m
$\widehat{\Delta}$	LES test filter width, m
Λ_w	wavelength of the sinusoidal profile at the bottom wall, m

Lower Greek symbols

α	amplitude-to-wavelength ratio, $2a/\Lambda_w$
β	volumetric thermal expansion coefficient, 1/K
λ	thermal conductivity, W/(m K)
λ_{ci}	measure of the swirling strength
ν	kinematic viscosity, m^2/s
ν_t	turbulent viscosity, m^2/s
ρ	fluid density, $\mathrm{kg/m}^3$
τ_w	wall shear stress, Pa
$\tau_{ij} =$	$\overline{u_i' u_j'}$ subgrid turbulent stress, $\mathrm{m}^2/\mathrm{s}^2$
$\tau_{\theta i} =$	$\overline{T' u_l'}$ subgrid turbulent heat flux, mK/s

Abbreviations

DNS	direct numerical simulation
LES	large eddy simulation
LIF	laser induced fluorescence
PIV	particle image velocimetry

Subscript and Superscript

b	bulk quantity
H	channel height (used as length scale)
w	wall quantity
$+$	wall-units

constant Reynolds numbers of Re = 125, 250, or 500, respectively. Their flow visualisation results showed that heat transfer enhancement for all cases is preceded by the onset of a secondary flow. Yu et al. [8], [9], carried out a numerical and experimental study to investigate this secondary flow in a mixed convective airflow through a horizontal plane channel at Reynolds number $\mathrm{Re} \leq 50$ and $3000 \leq \mathrm{Ra} \leq 10\,000$. Their results showed that this secondary flow is in the form of longitudinal vortex rolls, which changes to transverse rolls when the Reynolds number is lowered (or the Rayleigh number increased). For $\mathrm{Re} < 50$ they observed only transverse structures, i.e. that thermal buoyancy effects dominate the mean flow. Zhang et al. [10] addressed the flow patterns and heat transfer enhancement of mixed convective airflow in a rectangular channel at Re = 40 and $100 \leq \mathrm{Ra} \leq 4200$. Depending on the Rayleigh number they found two– (Ra = 100), four– ($\mathrm{Ra} \geq 630$), and six-roll ($\mathrm{Ra} \geq 1708$) modes of the longitudinal flow structures. Each roll mode produced significant heat transfer enhancement.

An interesting practical application was addressed in Alawadhi [11] where the convective cooling enhancement for rectangular blocks using a wavy plate was investigated. This problem is particularly important for the efficient cooling of the printed circuit board assembly. The two-dimensional numerical simulations were performed for different plate waviness at Reynolds numbers in a range of $250 \leq \mathrm{Re} \leq 1000$. The numerical simulation demonstrated that the wavy plate enhanced cooling of the rectangular blocks and reduced their surface temperature up to 25%.

The forced convective flow over a wavy wall in fully devolved turbulent flow regimes has been extensively studied in literature. In a direct numerical simulation (DNS) Cherukat et al. [12] addressed the characteristics of the developing shear layer above the recirculation zone formed after the wave crest of a wavy wall with an amplitude-to-wavelength ratio of $\alpha = 0.05$ at a Reynolds number of 3460 (defined with the bulk velocity and the half channel height). Large eddy simulations (LES) of forced convective wavy boundary flow were performed by Henn and Sykes [13], and Tseng and Ferziger [14]. In their extensive study Henn and Sykes [13] focused on the effects of different wave slopes ranging from 0 to 0.628 on turbulence at $5720 \leq \mathrm{Re} \leq 20\,060$.[2] They identified a scaling between the slope of small-amplitude waves and the velocity fluctuations, which is linear for the streamwise and vertical velocity components, but squared for the lateral. This is caused by the presence of coherent structures located at the upstream side of the wave. Tseng and Ferziger concentrated on these coherent structures for a wavy wall of $\alpha = 0.1$ at Re = 2400, and illustrated the vortex formation and transport of Görtler vortices induced by the local wall curvature.

The buoyancy driven convection from wavy surfaces was investigated by Krettenauer and Schumann [15] by means of a DNS, and by Hanjalić and Kenjereš [16] by means of T-RANS. Krettenauer and Schumann investigated Rayleigh numbers up to 4.5×10^4, and they observed that the flow features were not sensitive to alterations of the wavy surface. In their approach Hanjalić and Kenjereš investigated the same geometrical configuration at increased Rayleigh numbers up to $\mathrm{Ra} = 10^9$ and identified changes in the organisation of the coherent structures when advancing from two- to three-dimensional waviness. The forced convective flow over different wavy walls having amplitude-to-wavelength ratios of

[2] The wave slope is given by ak, with the wavenumber $k = 2\pi/\Lambda_w$.

0.01, 0.05, and 0.1 at a Reynolds number of Re = 6760 was addressed by Choi and Suzuki by means of LES [17]. An increase in heat transfer efficiency depending on the geometrical parameters of the wavy surface was observed. By changing the amplitude-to-wavelength ratios from 0.01 to 0.1 the Nusselt numbers increased by a factor of 4. This heat transfer enhancement is the topic of several other numerical works employing turbulence models addressing convective heat transfer in channel bound by one or two wavy walls (e.g. Dellil et al. [3], Metwally and Manglik [18]).

It is important to note that the great majority of previous experimental and numerical studies in literature focused on either forced or natural convection situations over wavy walls. The primary objective of our study is to fill this gap and to focus on the mixed convection case for the wavy wall configuration. Additional motivation lies in the possibility to perform a direct validation of the numerical simulations with recent experimental studies performed by the authors, Kuhn and Rudolf von Rohr, [19,20]. In the present numerical work we specifically address the influence of thermal buoyancy in the mixed convective flow over a wavy wall at different Richardson numbers (with the Reynolds number ranging from Re = 20 to Re = 2000). By performing a dynamic LES, we focused our investigations on the wall heat transfer and reorganisation of the flow structures.

2. Flow description

We consider the mixed convective flow between a flat top wall and a heated sinusoidal bottom surface. The bottom surface is characterised by the amplitude-to-wavelength ratio of $\alpha = 2a/\Lambda_w = 0.1$, having a wavelength of $\Lambda_w = 30$ mm which is equal to the channel height H. The profile of the wavy wall and the used coordinate system is depicted in Fig. 1. The computational domain has a streamwise and spanwise extension of one wavelength. This size is sufficient for the computation of flows over wavy walls and was verified by comparing isothermal LES results with available PIV measurements and the DNS of Maaß and Schumann [21] by Wagner [22]. The profile of the wavy wall is defined as:

$$y_w(x) = a\cos\left(\frac{2\pi x}{\Lambda_w}\right). \tag{2}$$

The mixed convective flow is characterised by the Reynolds number and the Rayleigh number. The Reynolds number Re is calculated according to

$$\mathrm{Re} = \frac{U_B H}{\nu}, \tag{3}$$

where ν denotes the kinematic viscosity, H is the height of the channel, and the bulk velocity U_B is given by

$$U_B = \frac{1}{H - y_w}\int_{y_w}^{H} U\left(x_\xi, y\right)dy, \tag{4}$$

where x_ξ denotes an arbitrary x-location and y_w describes the profile of the complex surface. The Rayleigh number Ra is given by

$$\mathrm{Ra} = \frac{gH^4\dot{q}\beta}{\nu^2\lambda}\mathrm{Pr}, \tag{5}$$

where $\dot{q}$ denotes the heat flux applied on the bottom wall, β is the volumetric thermal expansion coefficient, and Pr denotes the Prandtl number of the fluid. The fluid properties are given in Table 1. The details of the simulations reported in this paper are given in Table 2, where the characteristic numbers Re, Ra, and Ri for each simulated case are tabulated, together with the number of grid cells

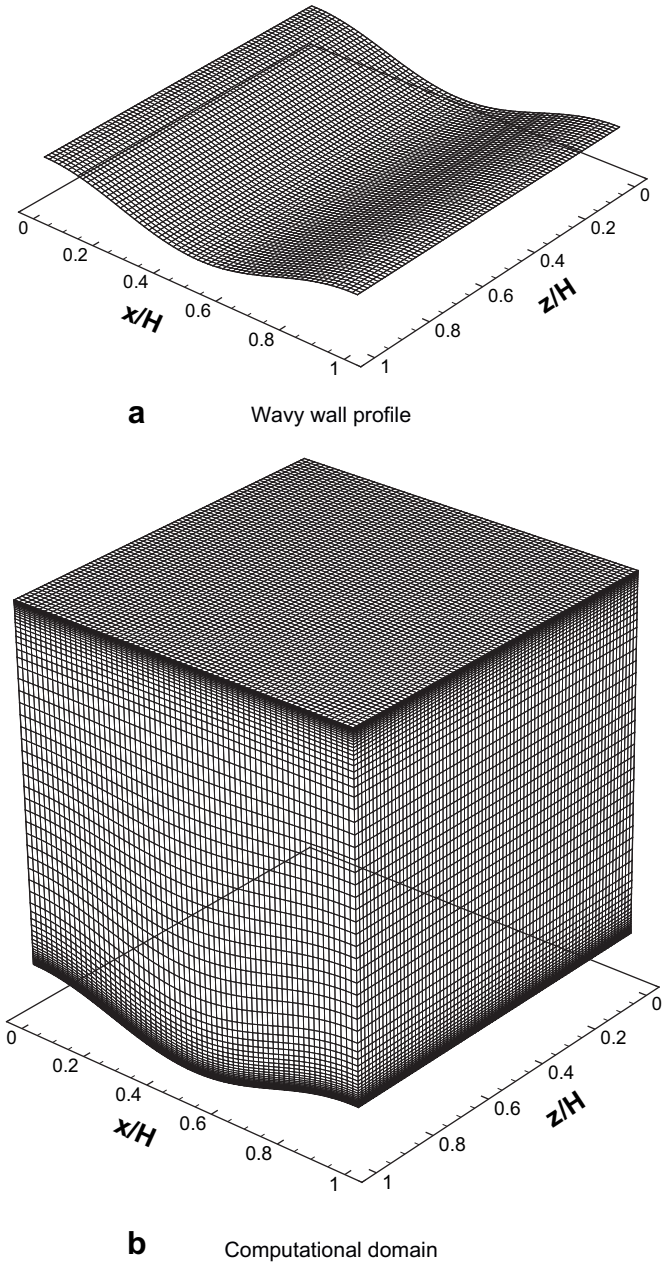

Fig. 1. Computational domain and profile of the wavy wall characterised by $\alpha = 0.1$ and $\Lambda_w = 30$ mm.

in each coordinate direction N_i and the dimensionless grid spacing (respectively the distance of the first grid point from the wall in the y-coordinate direction). The friction velocity u_τ to calculate all dimensions in wall-units was calculated from the wall shear stress τ_w, i.e.

Table 1
Properties of water at a temperature of $T = 20\ ^\circ$C [23].

Property	
Density ρ (kg/m^3)	1000
Kinematic viscosity ν (m^2/s)	1×10^{-6}
Thermal conductivity λ (W/(mK))	0.597
Heat capacity c_p (J/(kgK))	4186
Thermal expansion coefficient β (1/K)	2.07×10^{-4}
Prandtl number Pr	7

Table 2
Large eddy simulations of mixed convective flow over waves.

Re	Ra	Ri	N_x	N_y	N_z	Δx^+	y^+	Δz^+
20	1.4×10^7	5000	64	64	80	0.43	0.02	0.34
200	1.4×10^7	50	64	64	80	1.03	0.06	0.83
1000	1.4×10^7	2	64	64	80	1.88	0.11	1.50
2000	1.4×10^7	0.5	64	64	80	3.44	0.20	2.75

$$u_\tau = \sqrt{\frac{\tau_w}{\rho}}. \tag{6}$$

For the simulations we apply periodic boundary conditions in streamwise and spanwise direction by defining the total mass flux in streamwise direction through the domain. The top wall is kept at a constant temperature ($T = 20\ ^\circ\mathrm{C}$), on the bottom wall a constant heat flux boundary condition ($\dot{q} = 1800\ \mathrm{W/m^2}$) is imposed.

3. Subgrid models and numerical details

The equations describing turbulent flows and heat transfer are given by the conservation of mass, momentum and thermal energy. The spatially filtered form of the conservation of momentum equation can be written as

$$\frac{\partial(\rho\overline{u_i})}{\partial t} + \frac{\partial(\rho\overline{u_i}\overline{u_j})}{\partial x_j} = -\frac{\partial\overline{p}}{\partial x_i} + \frac{\partial}{\partial x_j}\left[\mu\frac{\partial(\rho\overline{u_i})}{\partial x_j} - \rho\tau_{ij}\right] + F_i, \tag{7}$$

and the conservation of thermal energy equation becomes

$$\frac{\partial(\rho\overline{T})}{\partial t} + \frac{\partial(\rho\overline{u_j}\overline{T})}{\partial x_j} = \frac{\partial}{\partial x_j}\left[\frac{\mu}{\mathrm{Pr}}\left(\frac{\partial\overline{T}}{\partial x_j}\right) - \rho\tau_{\theta j}\right], \tag{8}$$

where $\overline{p}$ is the filtered pressure field, F_i is an external force, μ denotes the dynamic viscosity of the fluid, Pr is the Prandtl number defined as $\mathrm{Pr} = \mu c_p/\lambda$, and τ_{ij}, $\tau_{\theta j}$ represent the unresolved turbulent stress and turbulent heat flux, respectively. The coupling between the temperature and the velocity fields is accomplished by applying the Boussinesq approximation:

$$F_B = -\rho g_i \beta(\overline{T} - T_{\mathrm{ref}}), \tag{9}$$

where β is the thermal expansion coefficient of the fluid, and g_i the acceleration due to gravity.

The large eddy simulations are performed by using the dynamic Smagorinsky model for the subgrid scales, Germano [24]:

$$\tau_{ij} - \frac{1}{3}\tau_{kk}\delta_{ij} = -2\nu_t\overline{S_{ij}}. \tag{10}$$

The eddy viscosity is defined as

$$\nu_t = (C_S\Delta)^2|\overline{S}|, \tag{11}$$

where Δ denotes the length scale of the unresolved motion calculated from the volume of the computational cell ΔV

$$\Delta = (\Delta V)^{1/3}, \tag{12}$$

and $|\overline{S}|$ is the magnitude of the strain rate defined as

$$|\overline{S}| = \sqrt{2\overline{S_{ij}}\,\overline{S_{ij}}},\ \overline{S_{ij}} = \frac{1}{2}\left(\frac{\partial\overline{u_i}}{\partial x_j} + \frac{\partial\overline{u_j}}{\partial x_i}\right) \tag{13}$$

C_S is evaluated from the dynamical procedure

$$C_S = -\frac{1}{2}\frac{L_{ij}M_{ij}}{M_{kl}M_{kl}}, \tag{14}$$

where $L_{ij} = \widehat{\overline{u_i}\,\overline{u_j}} - \widehat{\overline{u_i}}\,\widehat{\overline{u_j}}$ represents the resolved turbulent stress of the scales between Δ and a coarse $\hat{\Delta}$(where $\hat{\Delta} = 2\Delta$) , and $M_{ij} = \Delta^2\widehat{|\overline{S}|\overline{S_{ij}}} - \hat{\Delta}^2|\widehat{\overline{S}}|\widehat{\overline{S_{ij}}}$ represents the contribution of the modeled stress of those scales.

For the simulations a fully unstructured, finite-volume based second order accurate numerical code is used, Ničeno [25]. Collocated grid arrangement is used for all variables with Rhie–Chow interpolation and the SIMPLE algorithm for pressure-velocity coupling. Both, convective and diffusive terms of the discretised equations are approximated by a second-order central difference scheme (CDS). The time integration is performed by a fully implicit second-order three-consecutive time-steps method. The value of the characteristic time step is selected to ensure that at each particular time instant the value of $CFL_{\max} < 0.5$. The time averaging started after reaching a fully developed turbulent regime (usually reached after 4000 time steps, which corresponds to $\approx$ 14 flow through times through the domain) and continued for additional 30 000 time steps, which corresponds to $\approx$ 105 flow through times through the domain. This solver was previously extensively validated on numerous test cases involving fully developed channel and pipe flows, impinging jet and flow over an array of heated cubes, Ničeno [25], Hadžiabdić [26], Popovac [27], Hadžiabdić and Hanjalić [28].

Since the wavy surface geometry is easy to be represented, hexagonal control volumes are employed for the numerical mesh. The employed numerical mesh is refined in the proximity of the thermally active horizontal walls in order to fully resolve both hydrodynamical and thermal boundary layers. Details of the numerical mesh are provided in Table 2. The used numerical mesh was fully appropriate for the LES approach since the maximum of the ratio between subgrid turbulent and molecular viscosity for the highest value of Re = 2000 was below 0.5. This can be additionally confirmed by plotting vertical profiles of the ratio between the characteristic mesh size and the Kolmogorov length scale at $x/H = 0.5$, as shown in Fig. 2. It can be concluded that a well-resolved LES is achieved for all considered values of Re.

The dynamic procedure to obtain the Smagorinsky constant ensures correct near wall behaviour of the turbulent viscosity eliminating necessity to include the wall-damping functions (e.g. [29]).

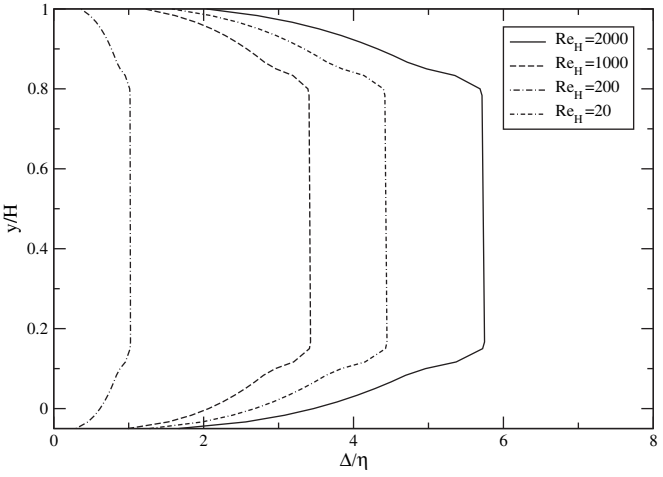

Fig. 2. Vertical profiles of the ratio between characteristic control volume ($\Delta = \Delta V^{1/3}$) and Kolmogorov ($\eta = (\nu^3/\varepsilon)^{1/4}$, $\varepsilon = \overline{u}^3_{max}/H$) length scales at the location $x/H = 0.5$, for Re = 20, 200, 1000, 2000, respectively.

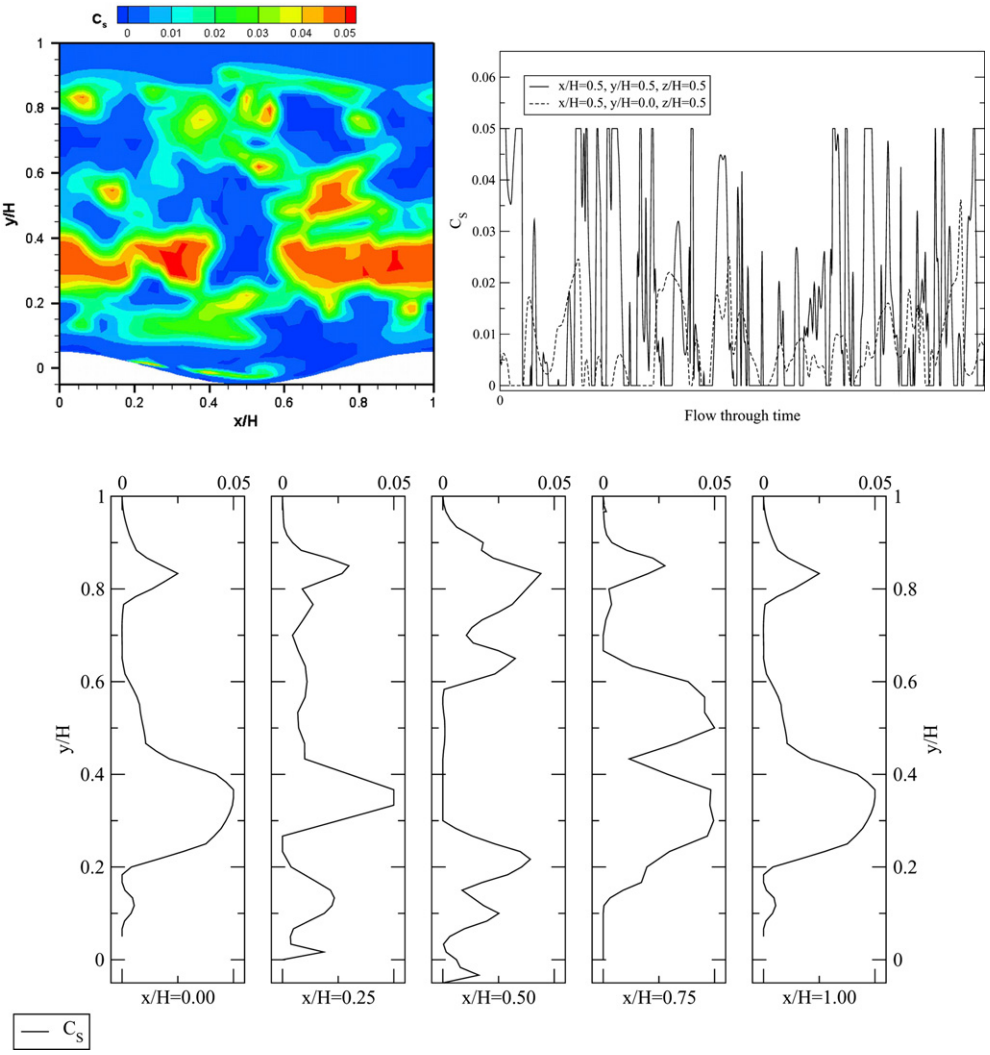

Fig. 3. Contours of the dynamic Smagorinsky constant C_S, profiles monitored at two different points in the flow field, and instantaneous vertical profiles of C_S along one wavelength, Re = 2000, Ra = 1.4×10^7.

Fig. 3-above shows contours of the Smagorinsky constant C_S at an arbitrary time instant together with its time-dependent behaviour at two characteristic monitoring points located in the centre of the simulated domain and in the proximity of the bottom wall, respectively. Similarly, the vertical profiles of C_S at different locations along the streamwise direction are shown in Fig. 3-below.

The subgrid turbulent heat flux is calculated from the simple gradient diffusion hypothesis as

$$\tau_{\theta i} = -\frac{\nu_t}{\mathrm{Pr}_t}\frac{\partial \overline{T}}{\partial x_i} \tag{15}$$

where $\mathrm{Pr}_t = 0.9$ is the turbulent Prandtl number.

4. Flow field

4.1. Velocity profiles and resolved turbulent stresses

In this section the influence of the different mixed convective regimes on the mean velocity profile in the (x, y)-plane is discussed. Therefore vertical velocity profiles at different streamwise locations x/H along the wavy surface are plotted, where $x/H = 0.00$ and $x/H = 1.00$ denote the wave crest, $x/H = 0.50$ the wave trough, and $x/H = 0.25$ and $x/H = 0.75$ the inflection point of the wall profile. To validate the numerical results the mean velocity profiles for Re = 1000 and 2000 are compared to measured data obtained by particle image velocimetry (PIV) of Kuhn et al. [30]. For a description of the experimental setup we refer to Günther and Rudolf von Rohr [31] and Kruse et al. [32], details about the applied measurement technique and the measurement procedure are found in Kuhn et al. [30] and Kuhn and Rudolf von Rohr [20]. Figs. 4 and 5 depict the comparison of the mean velocity profiles between PIV and LES at five different positions along the wavy wall for Re = 1000 and 2000, respectively. It can be seen that a good agreement between experiments and simulations are obtained for the streamwise velocity component at all locations. The vertical velocity component profiles show a similar good agreement with an exception for Re = 2000 at the positions $x/H = 0.75$, 1.0, where the LES profiles show higher values in comparison with the PIV data.

Fig. 6 shows the comparison of turbulent kinetic energy profiles obtained by PIV and LES at two streamwise positions representing the wave crest ($x/H = 0.00$) and the wave trough ($x/H = 0.50$), respectively, for Reynolds numbers Re = 1000 and 2000. The turbulent kinetic energy from LES is calculated only from the streamwise and vertical velocity fluctuations in order to resemble

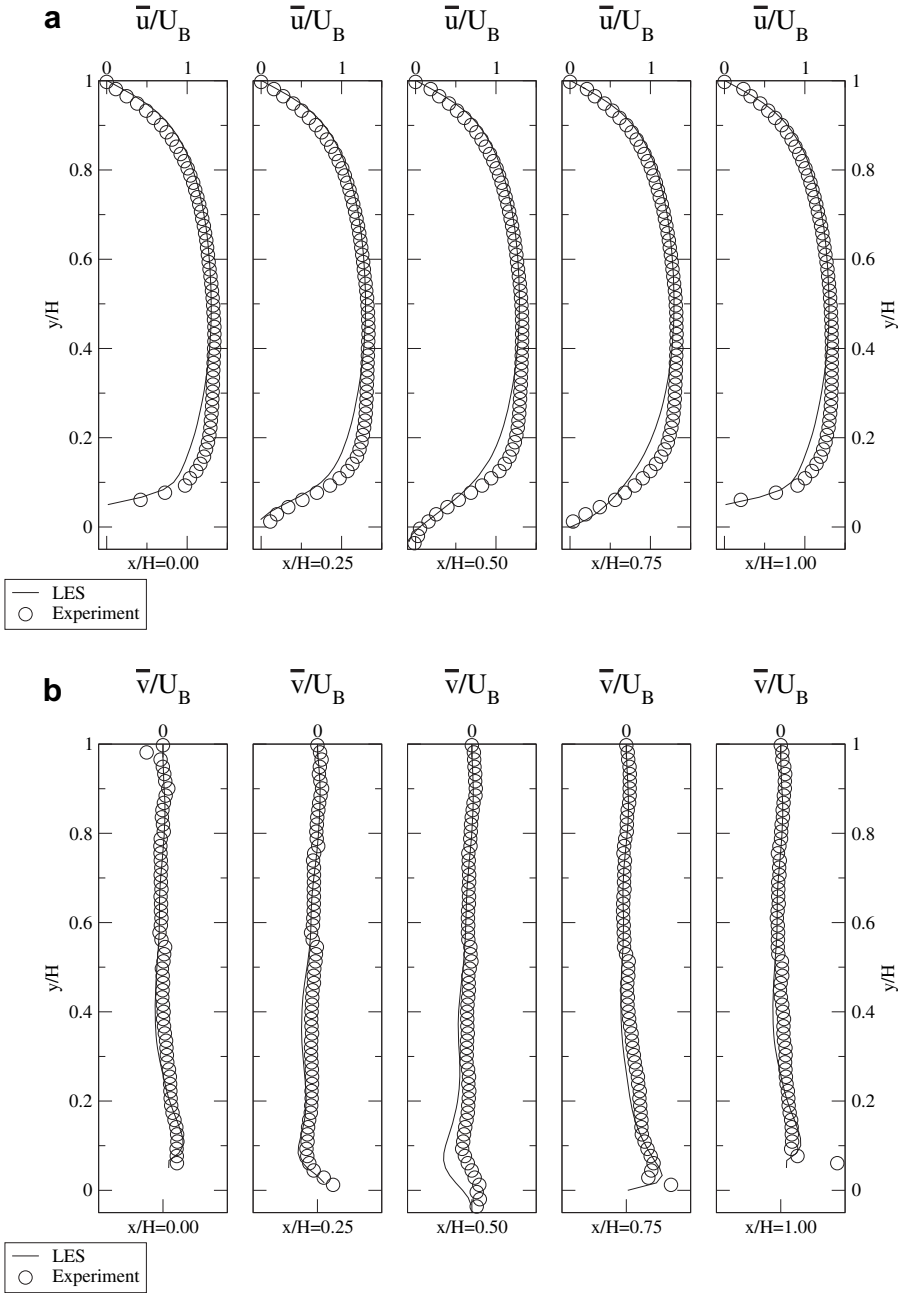

Fig. 4. Comparison of the mean velocity profiles between particle image velocimetry data and large eddy simulation of mixed convective flow over a wavy wall, Re = 1000, Ra = 1.4×10^7.

the two-dimensionality of the PIV data. It can be seen that for both values of Re the profiles exhibit a double peak behaviour (in the proximity of the top and bottom walls). For the lower value of Re = 1000 the peak value of turbulent kinetic energy from LES shows higher values and is moved closer to the wall – compared to the PIV data. At the identical locations and for the same Reynolds numbers, the vertical profiles of the turbulent shear stress are shown in Fig. 7. The agreement between the measured and computed profiles in the upper half of the channel ($0.50 \leq y/H \leq 1.00$) is good. However, deviations in the magnitude and peak locations are observed in the proximity of the heated bottom wall. This is the region that is strongly affected by thermal buoyancy effects. These differences between PIV and LES can be explained by a restricted ensemble size of the PIV measurements, together with measurement uncertainties caused by the changed optical properties of the fluid due to heating.[3]

To address the influence of the strength of the thermal buoyancy (from Re = 200 to 2000) on flow reorganisation, the mean streamwise velocity profiles are shown in Fig. 8. Negative values of the velocity at the streamwise position $x/H = 0.50$ found for all values of the Reynolds numbers indicate flow separation and the presence of a recirculation zone at the downstream side of the wave. For Re = 2000 the maximum flow velocity is found in the upper part of the channel ($y/H \approx 0.7$) which also results in an

[3] The statistical sample for combined PIV/LIF results was based on a number of 1000 images, while the LES statistics was based on 30 000 instantaneous fields.

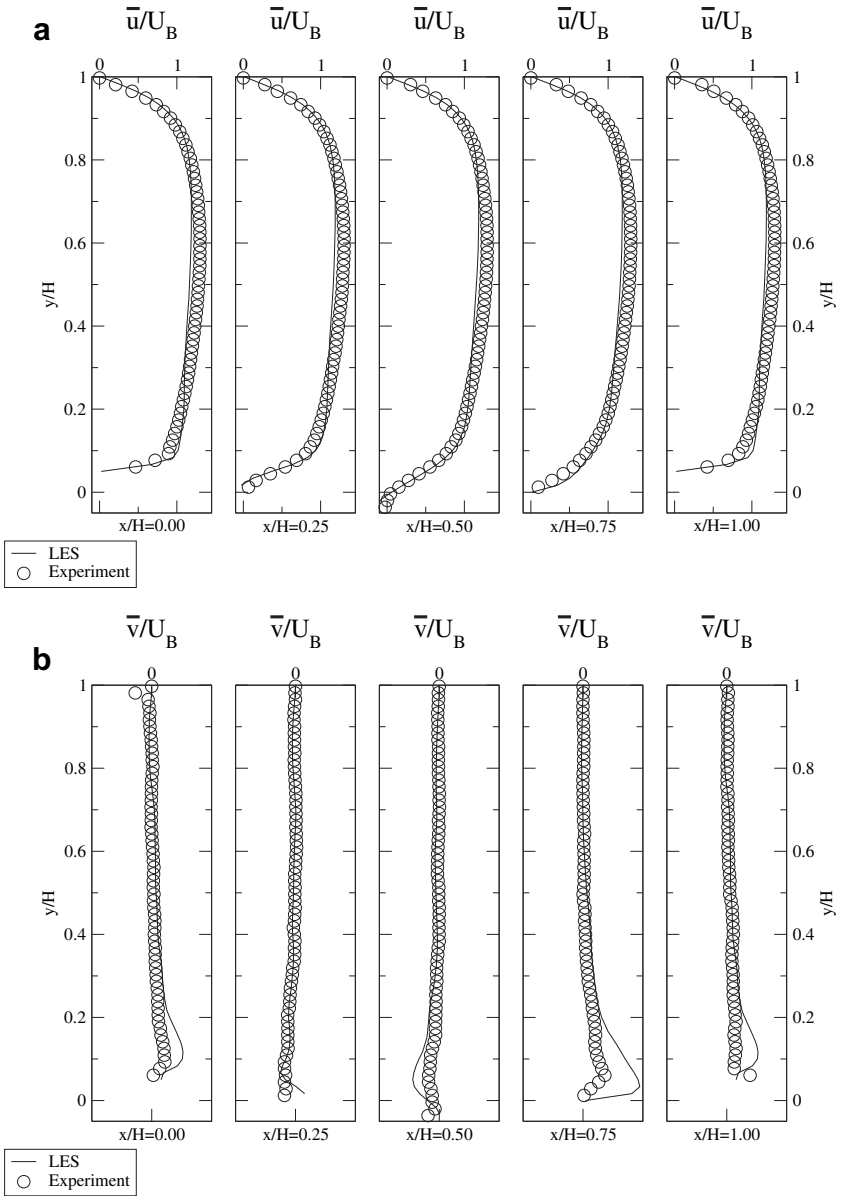

Fig. 5. Comparison of the mean velocity profiles between particle image velocimetry data and large eddy simulation of mixed convective flow over a wavy wall, Re = 2000, Ra = 1.4×10^7.

asymmetric profile. With decreasing Reynolds number, i.e. increasing impact of the natural convection, the location of the maximum flow velocity is shifted towards the heated surface. For Re = 1000 the velocity profile is symmetric with the velocity maximum in the centre of the channel. By further decreasing the Reynolds number the velocity profile is again asymmetric and the location of maximum fluid velocity is moved to $y/H \approx 0.15$ for Re = 200.

4.2. Turbulent kinetic energy, turbulence anisotropy and coherent structures

In order to identify the main production mechanism behind the turbulent mixing over a wavy wall, contours of the resolved turbulent kinetic energy $k = 0.5 \cdot (\overline{u'u'} + \overline{v'v'} + \overline{w'w'})$ for different values of Re = 20,…, 2000 in the central vertical plane ($z/H = 0.5$) are shown in Fig. 9. The values are non-dimensionalised by a characteristic mixed velocity defined as:

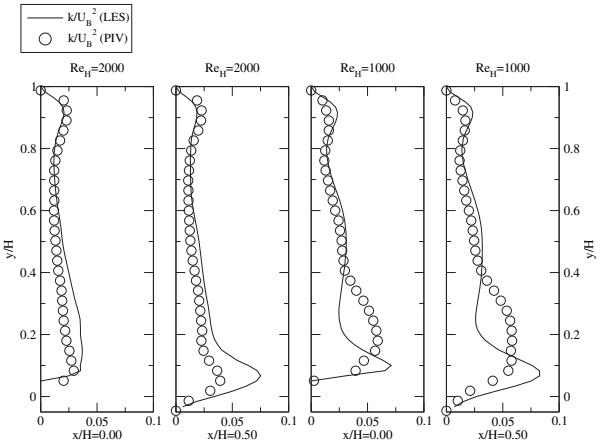

Fig. 6. Comparison of turbulent kinetic energy profiles ($k = 0.5 \cdot (\overline{u'u'} + \overline{v'v'})$) between PIV data and LES of mixed convective flow over a wavy wall at two streamwise positions for Re = 2000 (left) and Re = 1000 (right), Ra = 1.4×10^7.

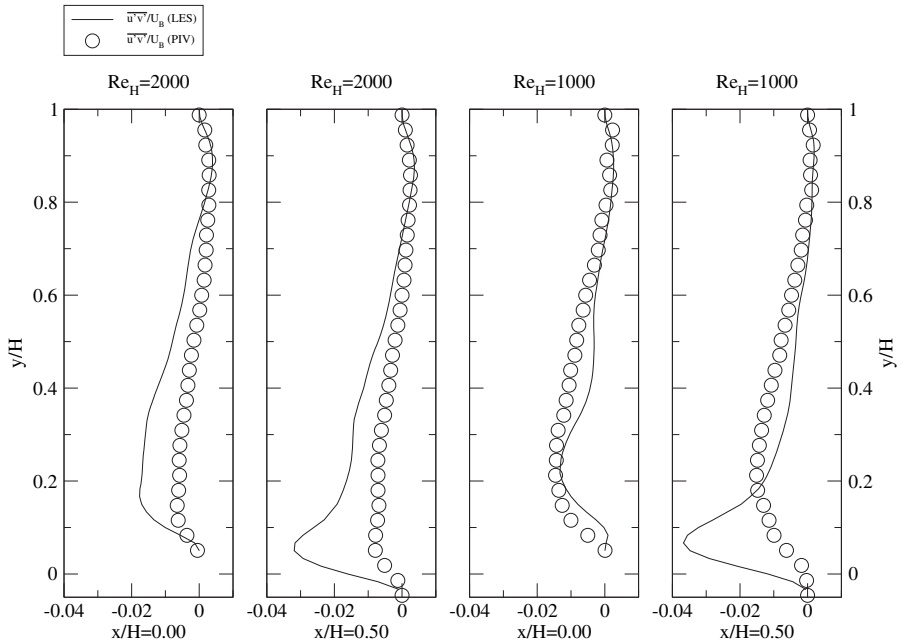

Fig. 7. Comparison of shear stress profiles between PIV data and LES of mixed convective flow over a wavy wall at two streamwise positions for Re = 2000 (left) and Re = 1000 (right), Ra = 1.4×10^7.

$$U_m = \sqrt{U_B^2 + U_{buoy}^2}, \tag{16}$$

where the buoyancy velocity U_{buoy} is calculated according to

$$U_{buoy} = \sqrt{\beta g \Delta T H}. \tag{17}$$

It can be seen that for Re = 20 the maximum of the resolved turbulent kinetic energy is identified in the central part of the domain above the wave crest. In this case, the major contribution of the turbulent kinetic energy comes from the thermal buoyancy production. For the intermediate value of Re = 200, the two distinct high turbulent kinetic energy regions are moved towards the centre of the simulated domain. For higher Reynolds numbers, Re = 1000 and 2000, the maximum values are observed in the proximity of the bottom wavy wall. Another approach to characterise the influence of the thermal buoyancy on the flow structures is to address the anisotropy of the flow, expressed by the anisotropy

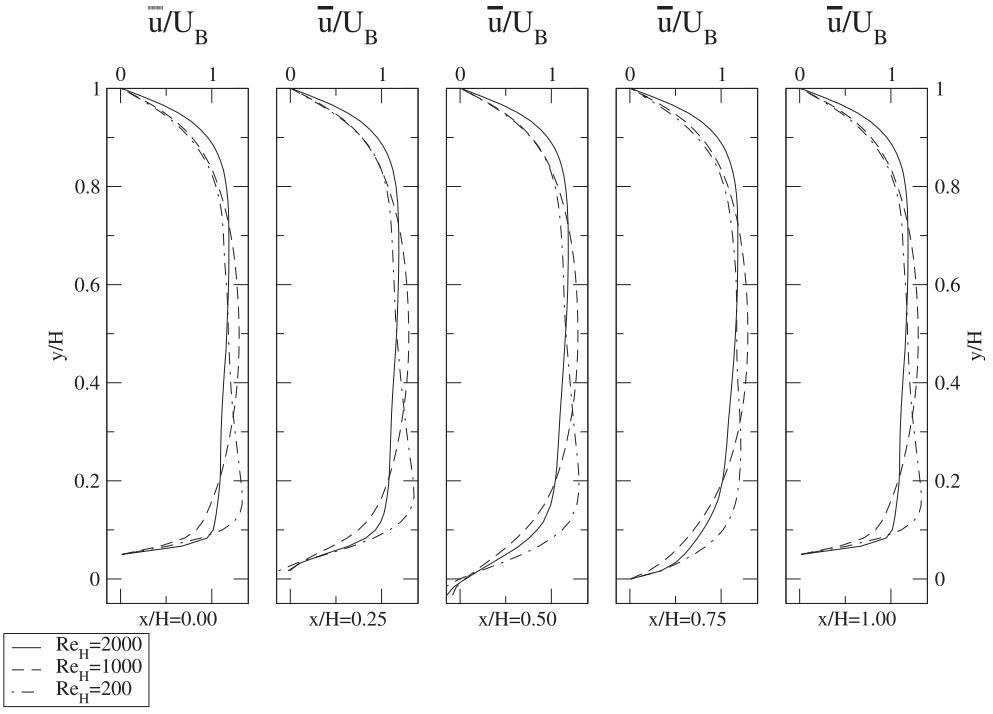

Fig. 8. Comparison of the normalised mean velocity $\overline{u}/U_B$ for Re = 200–2000, Ra = 1.4×10^7.

flatness parameter A, which is defined according to Lumley and Newman [33]:

$$A = 1 - \frac{9}{8}(A_2 - A_3), \tag{18}$$

where

$$A_2 = a_{ij}a_{ji}, \quad A_3 = a_{ij}a_{jk}a_{ki}, \quad a_{ij} = \frac{\overline{u_i'u_j'}}{k} - \frac{2}{3}\delta_{ij}. \tag{19}$$

Fig. 10 shows the contours of the flatness parameter A, which equals 1 for isotropic turbulence. It can be observed that this state of isotropic turbulence is reached in the centre of the flow channel for Reynolds numbers Re = 1000 and Re = 2000, similarly to the fully developed channel flow with flat walls. Low values of $A \approx 0$ near the wall for all four cases represent an increase in anisotropy due to the wall influence. For Re = 20 a region where $A \approx 0$ is also found just above the wave crest extending nearly over the entire channel height. This high level of the turbulence anisotropy is caused by a convective eddy (roll/cell structure) similar to the standard Rayleigh–Bénard convection situation. In order to visualise these eddy structures for different values of Re, the swirling strength criteria is used for their identification and extraction, Zhou et al. [34], Adrian et al. [35]. The swirling strength λ_{ci} is defined as the imaginary part of the complex eigenvalues of the local velocity gradient tensor. In a three-dimensional flow field the local velocity gradient tensor will have one real eigenvalue and a pair of complex conjugate eigenvalues when the discriminant of its characteristic equation is positive. When this is the case, the particle trajectories about the eigenvector corresponding to the real eigenvalue exhibit a spiral, swirling motion, Chong [36]. Fig. 11 shows the isosurfaces of constant swirling strength λ_{ci} for all considered Re. It is important to observe that these regions with strong swirling motion coincide very closely to the regions where the levels of turbulent anisotropy were highest. For the lowest value of Re = 20, the eddy structures are oriented with a central axis perpendicular to the mean flow – resembling closely convective Rayleigh–Bénard cells, Hanjalić and Kenjereš [37]. With further increase of the intensity of the inflow velocity, Re = 200, these eddy structures start to reorganise in a way that their central axis is now aligned with the flow in the streamwise direction. For the two highest values of Re = 1000, 2000, these large cell structures disappear and regions with intensive swirling can be observed only in the proximity of the wavy wall – portraying separation and recirculation zones, Fig. 11-below.

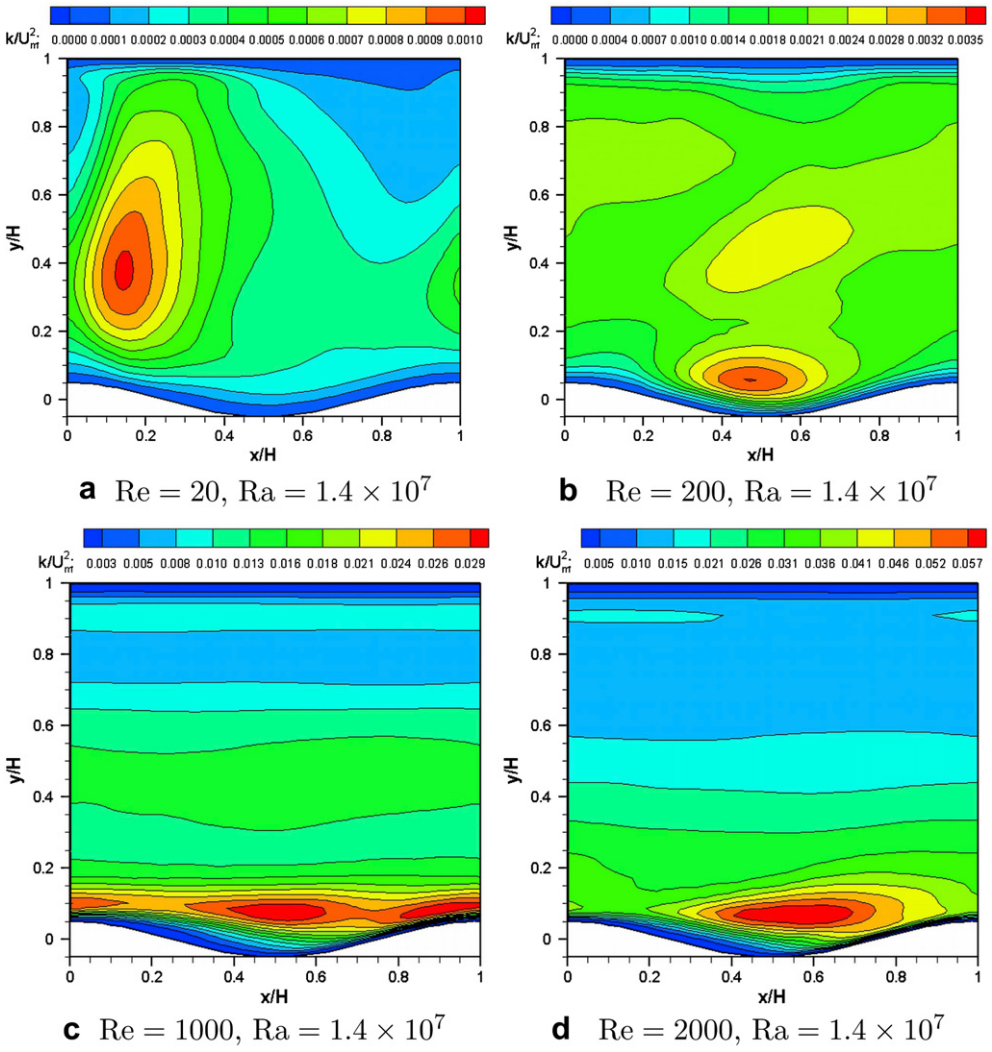

Fig. 9. Contours of turbulent kinetic energy k/U_m^2 for Re = 20, 200, 1000, 2000, Ra = 1.4×10^7.

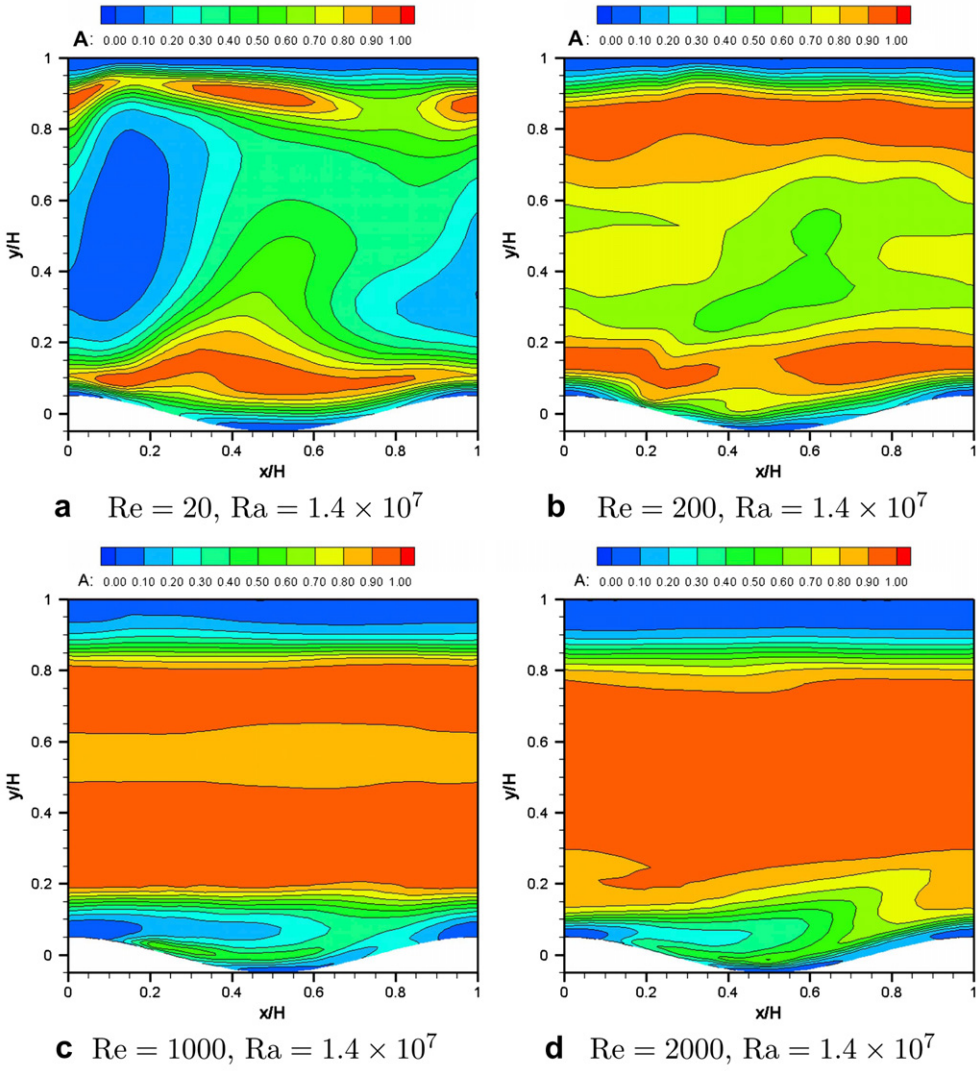

Fig. 10. Contours of the anisotropy flatness parameter A for Re = 2000, Re = 1000, Re = 200, and Re = 20; Ra = 1.4×10^7.

5. Scalar field

In this section we address the distribution of temperature as an active scalar and the influence of thermal buoyancy on the wall heat transfer.

5.1. Mean temperature and temperature variance

The vertical profiles of the mean temperature and temperature variance (normalised by a reference temperature) for Re = 1000, 2000 at two characteristic locations (x/H = 0, 0.5) are shown in Fig. 12. The LES results show generally good agreement with laser induced fluorescence (LIF) measurements for the mean temperature profiles for both values of Re at both locations. The only exception is the location x/H = 0.5 for Re = 2000, where the measured wall temperature is higher compared to the LES value. The temperature variance profiles show a good agreement in the proximity of the wavy wall, but significant deviations are observed in the proximity of the upper wall, Fig. 12b. Here, the LES profiles exhibit a proper near-wall behaviour since for the applied constant temperature boundary condition, the temperature variance should have a zero boundary value. In contrast to that, the measured profiles show a finite value at the wall indicating heat losses through this boundary during the experiment. In addition, due to the presence of the optical viewport for the measurements at the top wall light reflections occur which introduce an additional source of uncertainty, Kuhn and Rudolf von Rohr [20].

Contours of the mean temperature and temperature variance in the central vertical plane for different values of Re are given in Figs. 13–16. Also, the stream-traces are superimposed on the mean temperature field in order to illustrate the mutual dependency between the underlying velocity field with temperature distributions. It can be seen that the temperature variance reaches its maximum at the separation point. The locations of the separation and reattachment points for different values of Re are given in Table 3. The separation point moves from x_S/H = 0.1 to 0.16 for Re = 20 and 2000, respectively. For the same conditions, the reattachment point moves from x_R/H = 0.54 to 0.66. This behaviour indicates a horizontal shift and a vertical reduction of the re-circulative bubble. This is a consequence of the increasing forced convection influence over thermal buoyancy. It is interesting to compare these locations of separation and reattachment with a thermally neutral situation (no heating). In such a case, the separation points are located at x_S = 0.24, 0.19 and the reattachment points at x_R/H = 0.65, 0.72

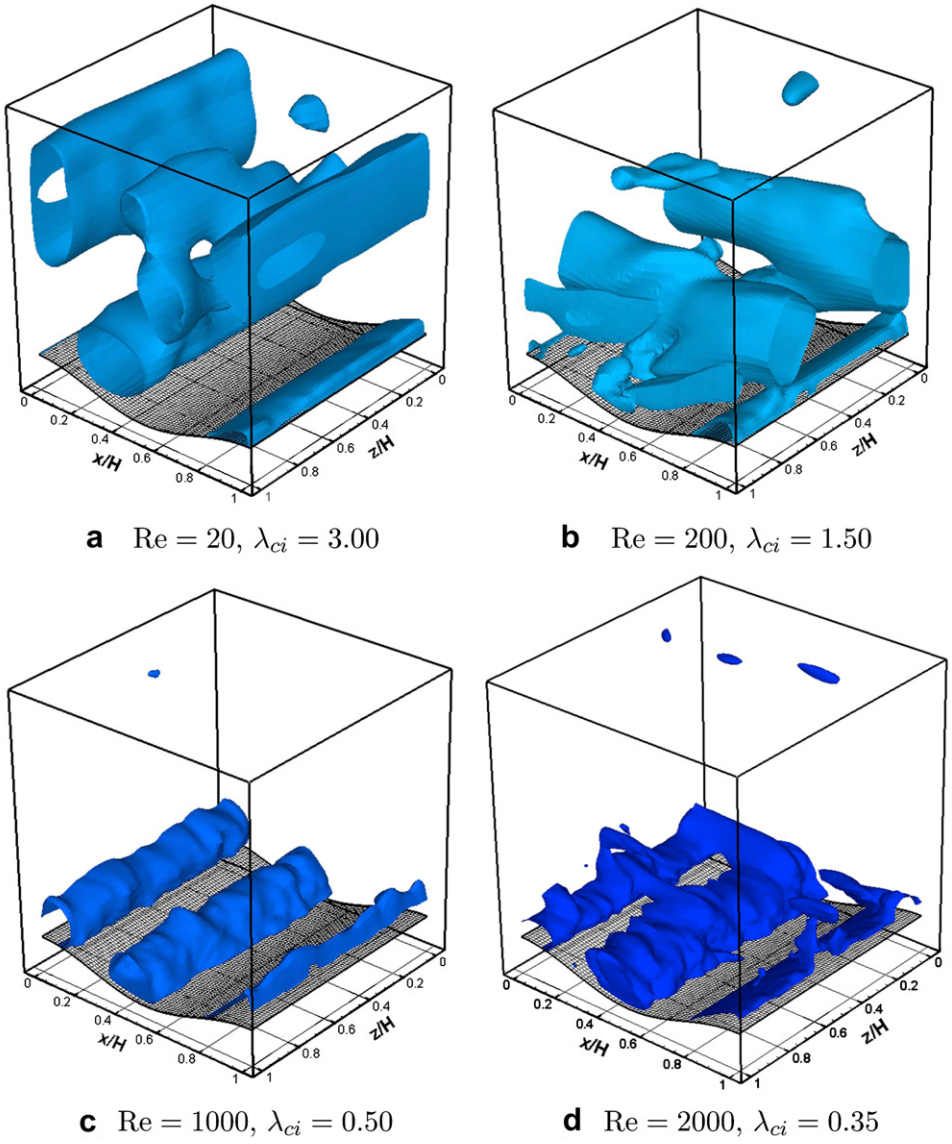

Fig. 11. Isosurfaces of constant swirling strength λ_{ci} for Re = 2000, Re = 1000, Re = 200, and Re = 20; Ra = 1.4×10^7.

for Re = 1000, 2000, respectively. These values obviously differ from the thermally active situations indicating that thermal buoyancy effects still play an important role for these two highest simulated values of Re.

5.2. Turbulent heat flux and wall heat transfer

Fig. 17 shows the comparison of the turbulent heat flux profiles between experimental and numerical data at two streamwise positions ($x/H = 0, 0.5$) for Re = 1000, 2000, respectively. As already stated for the velocity fluctuations, the agreement between the measured and computed profiles in the upper half of the channel ($0.50 < y/H < 1.00$) is good for Re = 2000. However, deviations in the magnitude and peak locations are observed in the region above the heated wall, where the thermal buoyancy is the most dominant. These differences between simulations and experiments can be explained by the restricted ensemble size of the PIV/LIF statistics together with measurement uncertainties. These uncertainties are caused by several sources, e.g. the changed optical properties of the fluid due to heating which affects the cross-correlation to calculate the velocity field, pulse-to-pulse variations in the laser intensity, inhomogeneities in the laser light sheet and laser light reflections in the field of view. This nicely demonstrates the importance of combined numerical simulation and experimental research in investigating complex turbulent mixed convection cases where many limitations of an experimental approach can be revealed. Contours of the horizontal and vertical turbulent heat flux components are shown in Figs. 18–21. For the case Re = 20 the vertical component of the turbulent heat flux vector is significantly larger in comparison to the horizontal component. It is interesting to observe that, for this situation, the highest value of the vertical turbulent heat flux does not coincide with the location of the strong recirculation but is concentrated in a region bordered by the already identified and discussed coherent structures, Fig. 11. In contrast to this situation, for higher values of Re, the horizontal heat flux component takes over the vertical component. The highest values of the vertical turbulent flux are concentrated in the region above the recirculation zones, Fig. 21.

The wall heat transfer, characterised by a local Nusselt number distribution, is presented next. We define the Nusselt number as

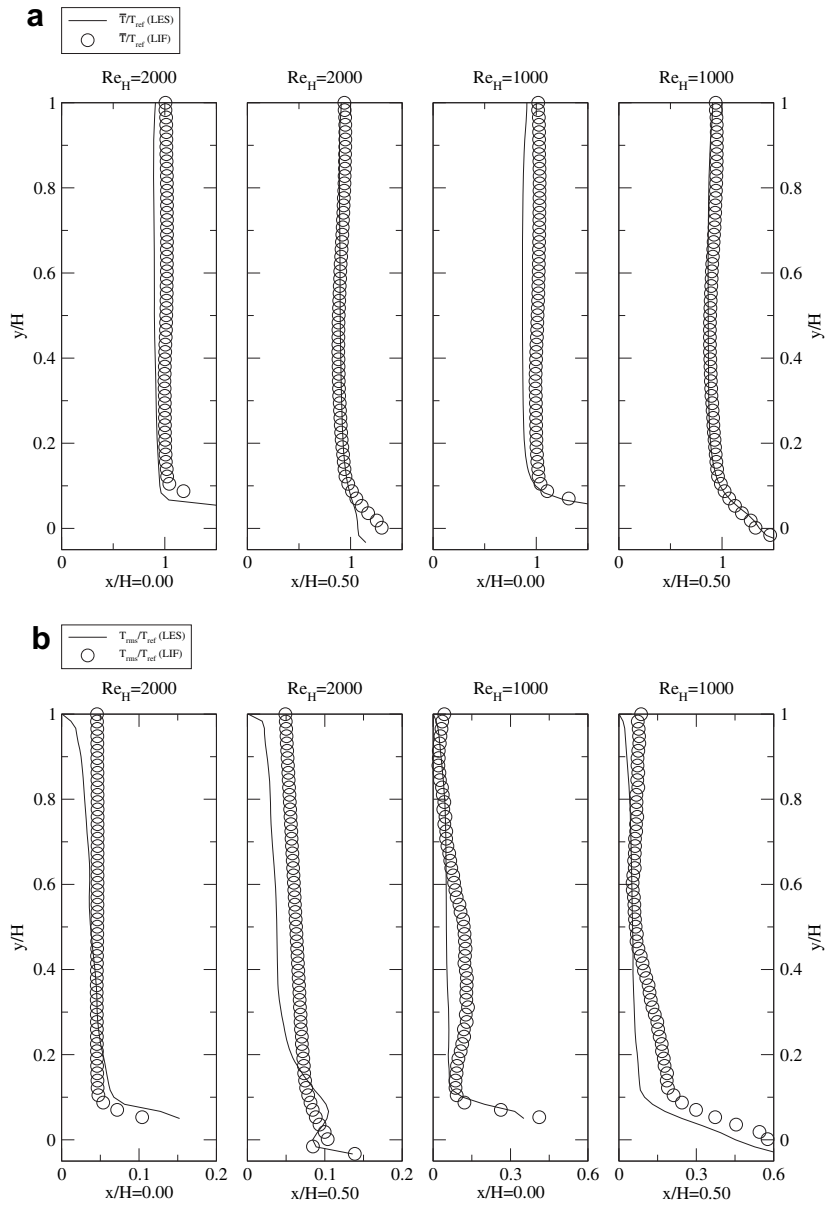

Fig. 12. Comparison of the mean temperature profiles and the temperature variance between LIF and LES at two streamwise positions for Re = 1000 and Re = 2000, Ra = 1.4×10^7.

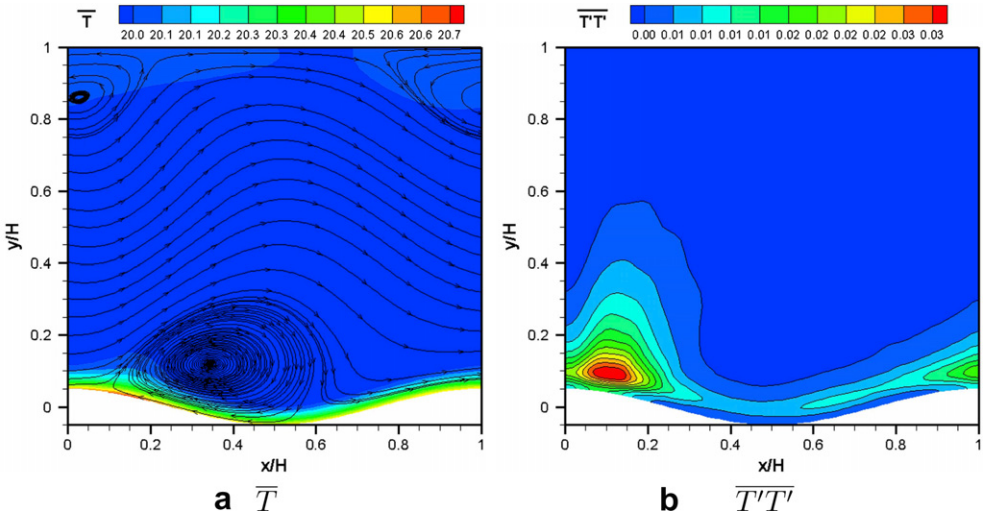

Fig. 13. Mean temperature with superimposed streamlines (-left) and temperature variance contours (-right), Re = 20, Ra = 1.4×10^7.

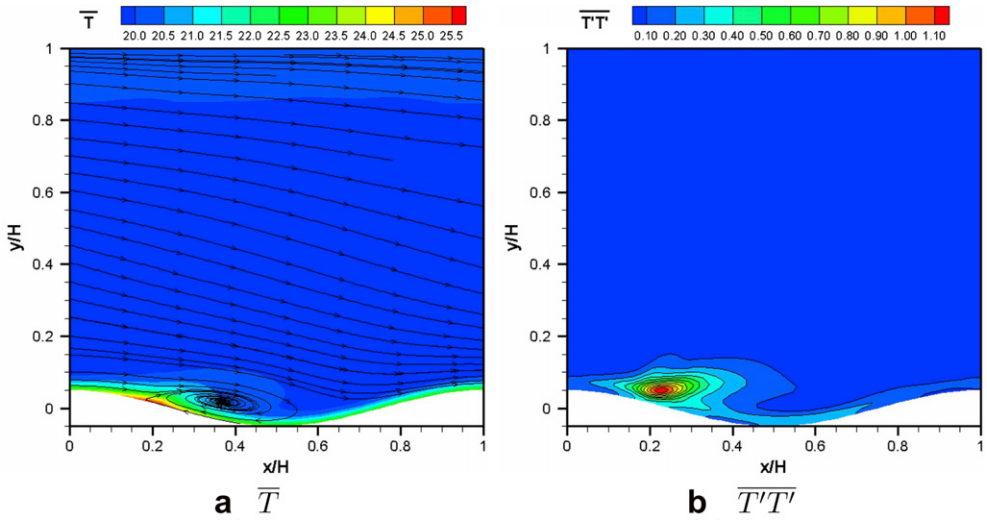

Fig. 14. Mean temperature with superimposed streamlines (-left) and temperature variance contours (-right), Re = 200, Ra = 1.4×10^7.

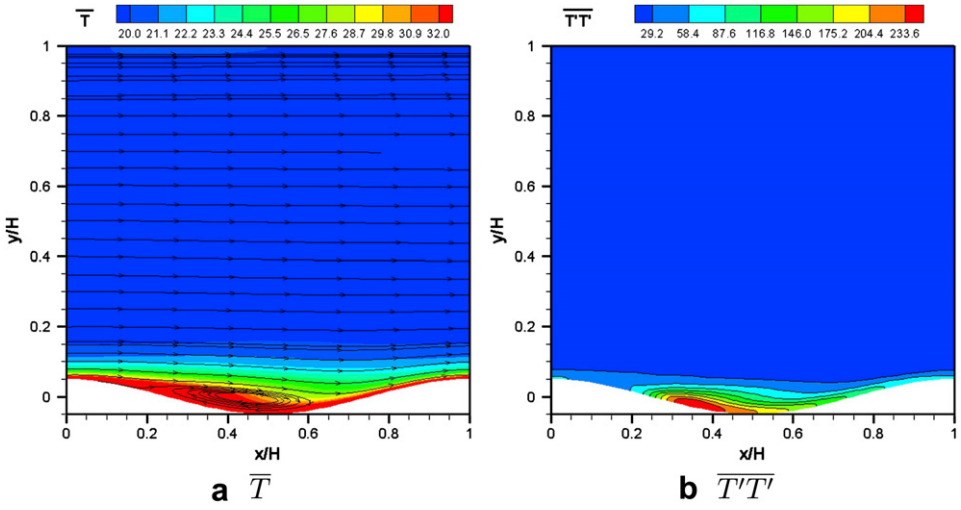

Fig. 15. Mean temperature with superimposed streamlines (-left) and temperature variance contours (-right), Re = 1000, Ra = 1.4×10^7.

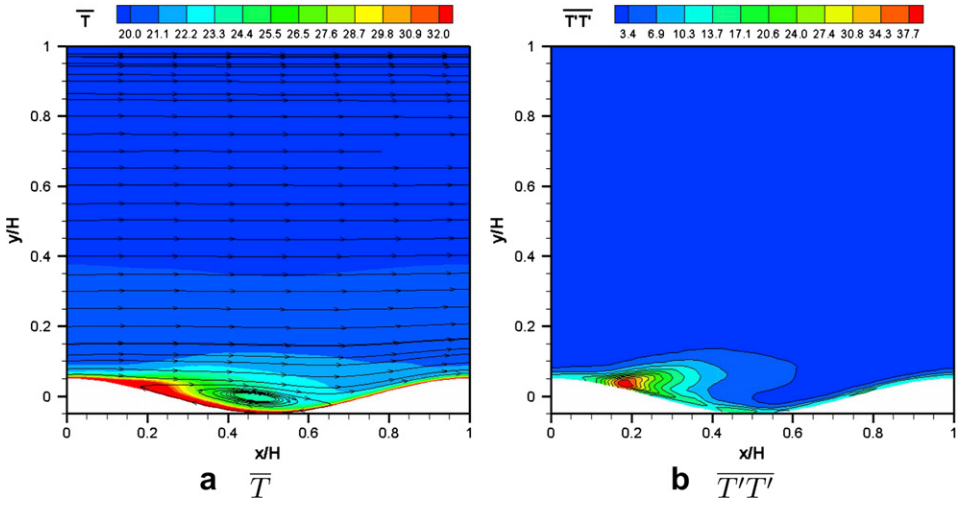

Fig. 16. Mean temperature with superimposed streamlines (-left) and temperature variance contours (-right), Re = 2000, Ra = 1.4×10^7.

Table 3
Coordinates of the point of separation x_S and reattachment x_R.

Re	Ra	Ri	x_S/H	x_R/H
20	1.4×10^7	5000	0.10	0.54
200	1.4×10^7	50	0.18	0.60
1000	1.4×10^7	2	0.18	0.65
2000	1.4×10^7	0.5	0.16	0.66

ratio between the total heat flux and the conductive heat flux, which reads

$$\mathrm{Nu} = \frac{\dot{q}H}{\lambda(T - T_{ref})} + 1. \tag{20}$$

Fig. 22 shows the contours of the Nusselt number at the heated surface for all Reynolds numbers ($\mathrm{Ra} = 1.4 \times 10^7$). The wave-averaged Nusselt numbers for each case are tabulated in Table 4. In general, an increase of the Nusselt number with increasing

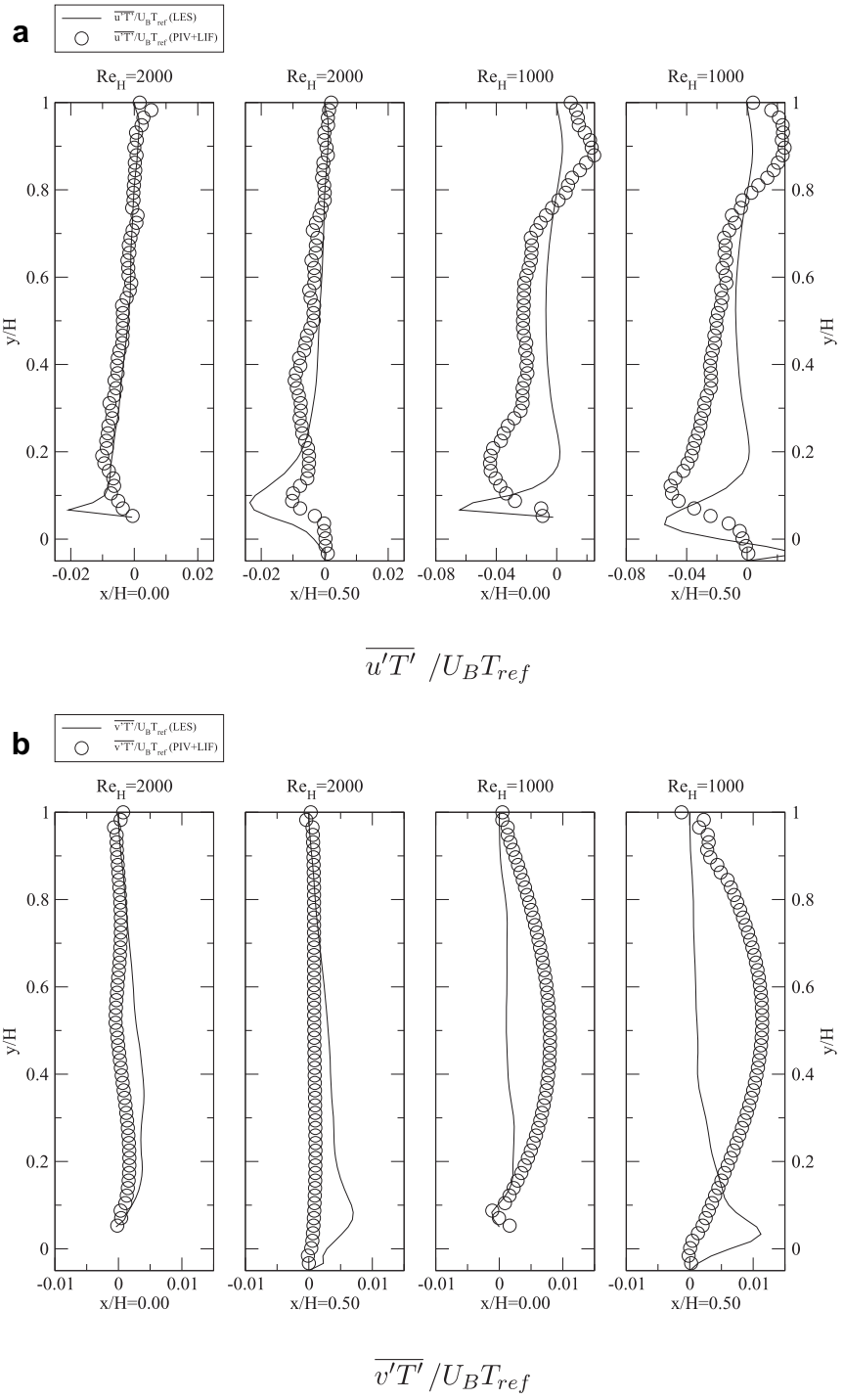

Fig. 17. Comparison of the turbulent heat flux profiles between combined PIV/LIF LES for Re = 1000 and Re = 2000, $\mathrm{Ra} = 1.4 \times 10^7$.

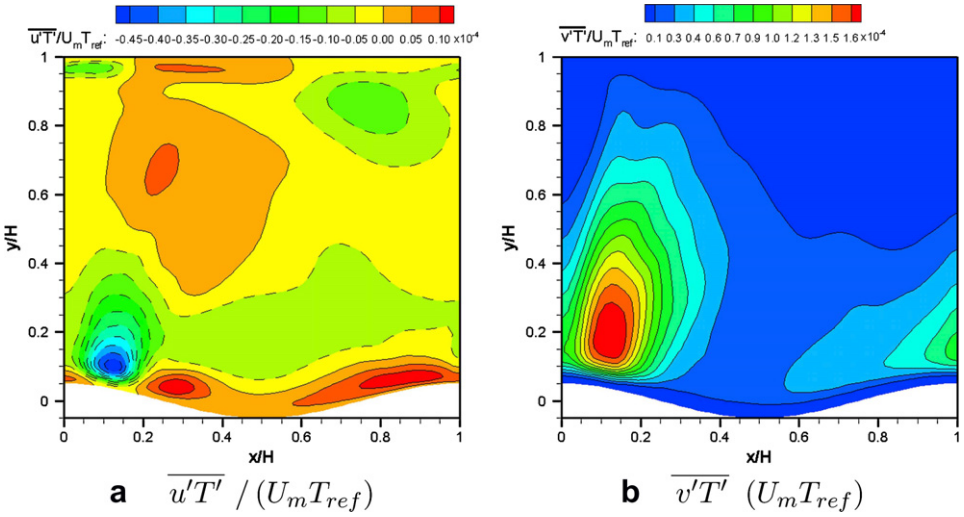

Fig. 18. Contours of horizontal and vertical heat flux, Re = 20, Ra = 1.4×10^7.

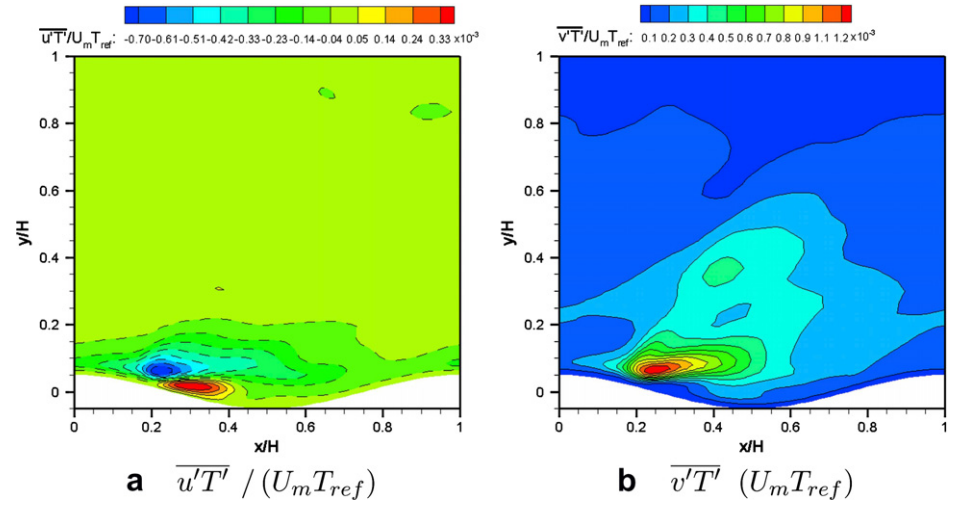

Fig. 19. Contours of horizontal and vertical heat flux, Re = 200, Ra = 1.4×10^7.

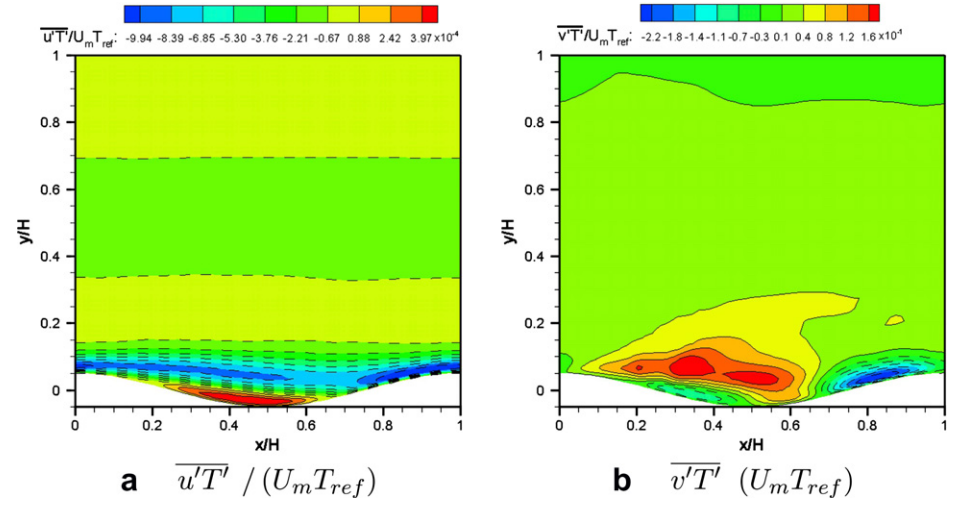

Fig. 20. Contours of horizontal and vertical heat flux, Re = 1000, Ra = 1.4×10^7.

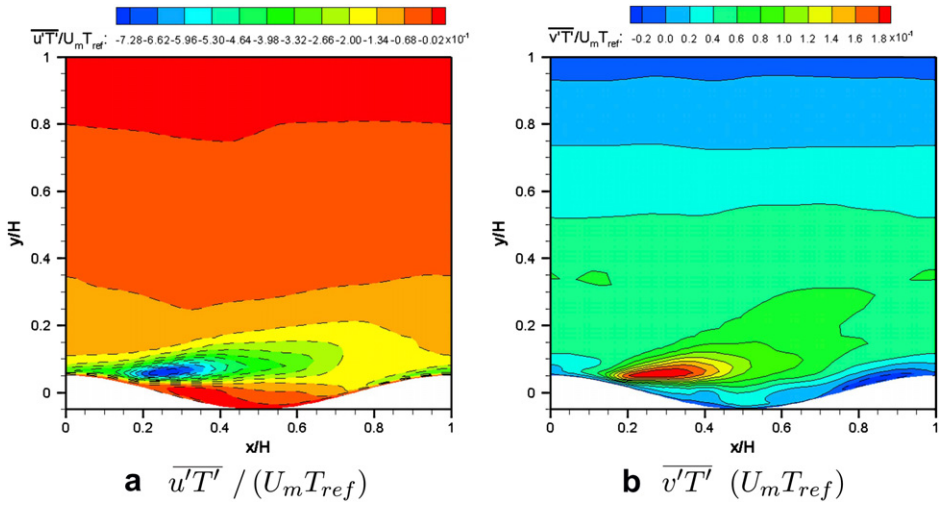

Fig. 21. Contours of horizontal and vertical heat flux, Re = 2000, Ra = 1.4×10^7.

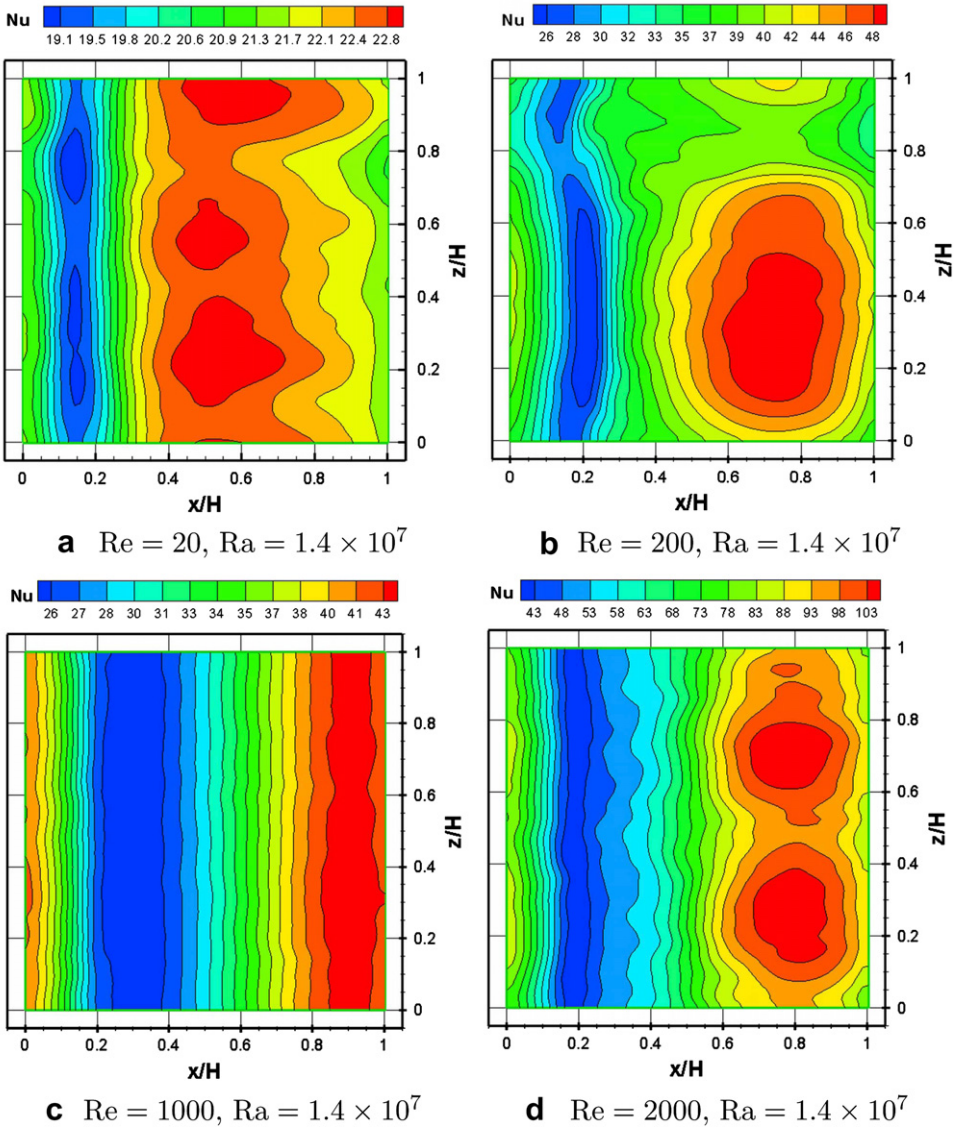

Fig. 22. Contours of the Nusselt number Nu for Re = 2000, Re = 1000, Re = 200, and Re = 20; Ra = 1.4×10^7.

Table 4
Comparison of mean Nusselt numbers with experiments and predictions for forced and free convection.

Re	Ra	Nu_{LES}^{mixed}	Nu_{exp}^{mixed}	Nu_{exp}^{forced}	Nu_{exp}^{free}
20	1.4×10^7	21.70	–	–	17.75
200	1.4×10^7	39.03	–	–	–
1000	1.4×10^7	34.02	36.00	15.29	–
2000	1.4×10^7	75.37	90.00	28.05	–

Reynolds number is observed. However, an interesting transition occurs between Re = 200 and 1000. It can be seen that the averaged value of the Nusselt number is higher for the smaller value of Re. This can be explained by an active role of the coherent structures in transporting mass, momentum and heat. For the smaller value of Re, these structures extend over the entire domain, i.e. they are not confined to the recirculation areas only, as shown in Fig. 11. In addition to heat transfer enhancement, these coherent structures also cause a strong non-uniformity of the wall heat transfer. This can be easily observed by comparing the imprints of these structures on the local heat transfer, Fig. 22b and c. It can be seen that for the lower value of Re = 200 a strong asymmetry in the local heat transfer distribution is present.

In the next section the integral heat transfer from the wavy surface is analysed. Therefore a comparative assessment of numerically obtained results with experimental data is performed. The experimental data include the recently conducted mixed convection measurements over wavy walls, Kuhn and Rudolf von Rohr, [19,20], as well as the experiments performed in purely forced, Gnielinski [38], or free convection flow regimes, Chu and Goldstein [39]. It is important to mention that the latter two experimental studies in purely free or forced convection were performed in configurations with a flat horizontal wall. By comparing our numerical results with these experimental studies, some important conclusions about the effects of the imposed wavy wall on the integral heat transfer can be made. Compared with the experimental correlation of Chu and Goldstein [39],

$$Nu_{exp}^{free} = 0.183\,Ra^{0.278}, \tag{21}$$

the LES result for Re = 20 shows a good agreement. The observed difference of 20% heat transfer enhancement is due to wall waviness. In contrast to that, compared with the pure forced convection experimental correlation (where the thermal buoyancy effects are neglected) of Gnielinski [38],

$$Nu_{exp}^{forced} = 0.037\,Re^{0.8}Pr/(1 + 2.443\,Re^{-0.1}(Pr^{2/3} - 1)), \tag{22}$$

the LES results show a significant heat transfer enhancement of factor 2.2 and 2.68 for at Re = 1000 and 2000, respectively. Finally, when compared to experiments in identical conditions (mixed convection and wavy horizontal wall, Nu_{exp}^{mixed}, Kuhn and Rudolf von Rohr [20]) the LES results show a good agreement at Re = 1000 and 2000. The difference for Re = 1000 is just about 2% while for the higher value of Re = 2000 an under-prediction of 16% is obtained. This difference in the Nusselt number can be explained by the different averaging procedures to compute the mean Nusselt number. The Nusselt number in LES is obtained by averaging over the whole simulated wavy surface (3D), i.e. the local patterns of the Nusselt number are taken into account. In contrast to that the experimentally obtained Nusselt number is averaged along the line of measurement (2D), i.e. the patterns of the Nusselt number caused by the flow organisation (e.g. see Fig. 22d) are not taken into account and thus the result differs from the non-homogeneous numerical solution.

6. Conclusions

In this paper we addressed the mixed convective flow over a heated wavy surface by means of a dynamic LES. The simulations covered a range of Reynolds and Richardson numbers, $20 \le Re \le 2000$ and $0.5 \le Ri \le 5000$, including transitional and turbulent flow regimes. Both, first and second order resolved velocity statistics show a good agreement with experimental PIV data of Kuhn and Rudolf von Rohr [19,20]. Simulations also revealed some inconsistencies in measured temperature variance and turbulent heat flux profiles. This indicates that further improvements of the combined PIV/LIF experimental approach are needed. The vortical flow structures are identified and visualised by applying the swirling intensity criteria. An interesting spatial flow reorganisation takes place between Re = 20 and 200, when spanwise oriented rolls start to be aligned in the streamwise direction. Next to causing a significant turbulence anisotropy in the central part of the considered flow domain, the wall imprints of these vortical structures can also be identified in the distributions of the local heat transfer. Predicted values of the integral Nusselt numbers show a good agreement with recent experimental studies of mixed convection for Re = 1000, 2000. A good agreement is also obtained for a pure free convection experimental correlation for low Re = 20. Compared to a standard experimental Nusselt number correlation for forced convection over a flat wall, significant enhancements in heat transfer have been obtained – 2.2 and 2.68 times for Re = 1000 and 2000, respectively.

Acknowledgement

We gratefully acknowledge financial support from the Swiss National Science Foundation (SNF). The numerical work was carried out at TU Delft under the HPC-EUROPA project (RII3-CT-2003-506079), with the support of the European Community – Research Infrastructure Action under the FP6 'Structuring the European Research Area' Programme. Saša Kenjereš acknowledges the ERCOFTAC Leonhard Euler Centre visitor fellowships during 2003–2005 visits at the Institute of Process Engineering, ETH Zurich.

References

[1] M. Banna, L. Pietri, B. Zeghmati, Turbulent mixed convection of heat and water vapor transfers in a two-dimensional vegetation canopy. Heat Mass Transf. 40 (2004) 757–768.
[2] T.A. Rush, T.A. Newell, A.M. Jacobi, An experimental study of flow and heat transfer in sinusoidal wavy passages. Int. J. Heat Mass Transf. 42 (1999) 1541–1553.
[3] A.Z. Dellil, A. Azzi, B.A. Jubran, Turbulent flow and convective heat transfer in a wavy wall channel. Heat Mass Transf. 40 (2004) 793–799.
[4] F.P. Incropera, D.P. DeWitt, Fundamentals of Heat and Mass Transfer. John Wiley & Sons, 2002.
[5] D.G. Osborne, F.P. Incropera, Laminar, mixed convection heat transfer for flow between horizontal plates with asymmetric heating. Int. J. Heat Mass Transf. 28 (1985) 207–217.
[6] D.G. Osborne, F.P. Incropera, Experimental study of mixed convection heat transfer for transitional and turbulent flow between horizontal, parallel plates. Int. J. Heat Mass Transf. 28 (7) (1985) 1337–1344.
[7] J.R. Maughan, F.P. Incropera, Regions of heat transfer enhancement for laminar mixed convection in a parallel plate channel. Int. J. Heat Mass Transf. 33 (1989) 555–570.
[8] C.H. Yu, M.Y. Chang, T.F. Lin, Structures of moving transverse and mixed rolls in mixed convection of air in a horizontal plane channel. Int. J. Heat Mass Transf. 40 (2) (1997) 333–346.
[9] C.H. Yu, M.Y. Chang, C.C. Huang, T.F. Lin, Unsteady vortex roll structures in a mixed convective air flow through a horizontal plane channel: a numerical study. Int. J. Heat Mass Transf. 40 (3) (1997) 505–518.
[10] H. Zhang, X.Y. Huang, H.S. Li, L.P. Chua, Flow patterns and heat transfer enhancement in low-Reynolds-Rayleigh-number channel flow. Appl. Therm. Eng. 22 (2002) 1277–1288.
[11] E.M. Alawadhi, Forced convection cooling enhancement for rectangular blocks using a wavy plate. IEEE Trans. Components Packaging Technologies 28 (2005) 525–533.

[12] P. Cherukat, Y. Na, T.J. Hanratty, J.B. McLaughlin, Direct numerical simulation of a fully developed turbulent flow over a wavy wall. Theor. Comput. Fluid Dyn. 11 (1998) 109–134.
[13] D.S. Henn, R.I. Sykes, Large-eddy simulation of flow over wavy surfaces. J. Fluid Mech. 383 (1999) 75–112.
[14] Y.-H. Tseng, J.H. Ferziger, Large-eddy simulation of turbulent wavy boundary flow – illustration of vortex dynamics. J. Turbulence 5 (034) (2004) 1–23.
[15] K. Krettenauer, U. Schumann, Direct numerical simulation of thermal convection over a wavy surface. Meteorol. Atmos. Phys. 41 (1989) 165–179.
[16] K. Hanjalić, S. Kenjereš, 'T-RANS' simulation of deterministic eddy structure in flows driven by thermal buoyancy and Lorentz force. Flow, Turbul. Combust. 66 (2001) 427–451.
[17] H.S. Choi, K. Suzuki, Large eddy simulation of turbulent flow and heat transfer in a channel with one wavy wall. Int. J. Heat Fluid Flow 26 (2005) 681–694.
[18] H.M. Metwally, R.M. Manglik, Enhanced heat transfer due to curvature-induced lateral vortices in laminar flows in sinusoidal corrugated-plate channels. Int. J. Heat Mass Transf. 47 (2004) 2283–2292.
[19] S. Kuhn, P. Rudolf von Rohr, Experimental investigation of mixed convective flow over a wavy wall. Int. J. Heat Fluid Flow 29 (2008) 94–106.
[20] S. Kuhn, P. Rudolf von Rohr, Experimental study of heat flux in mixed convective flow over solid waves. Exp. Fluids 44 (2008) 973–984.
[21] C. Maaß, U. Schumann, Flow Simulation with High Performance Computers. Vieweg, Braunschweig, 1996, Ch. Direct numerical simulation of separated turbulent flow over a wavy boundary, pp. 227–241.
[22] C. Wagner, Transport phenomena in complex turbulent flows: numerical and experimental methods, Ph.D. thesis, ETH Zurich, Switzerland, 2007.
[23] W. Wagner, A. Kruse, Properties of Water and Steam The industrial standard IAPWS-IF97 for thermodynamic properties and supplementary equations for other properties. Springer Verlag, Berlin, 1998.
[24] M. Germano, U. Piomeli, P. Moin, W.H. Cabot, A dynamic subgrid-scale eddy viscosity model. Phys. Fluids A 3 (1991) 1760–1765.
[25] B. Ničeno, An unstructured parallel algorithm for large eddy and conjugate heat transfer simulations, Ph.D. thesis, TU Delft, 2001.
[26] M. Hadžiabdić, Les, RANS and combined simulation of impinging flows and heat transfer, Ph.D. thesis, TU Delft, 2006.
[27] M. Popovac, Modeling and simulation of turbulence and heat transfer in wall-bounded flows, Ph.D. thesis, TU Delft, 2006.
[28] M. Hadžiabdić, K. Hanjalić, Vortical structures and heat transfer in a round impinging jet. J. Fluid Mech. 596 (2008) 221–260.
[29] E.R. van Driest, On turbulent flow near a wall. J. Aero. Sci. 23 (1956) 1007–1011.
[30] S. Kuhn, C. Wagner, P. Rudolf von Rohr, Influence of wavy surfaces on coherent structures in a turbulent flow. Exp. Fluids 43 (2007) 251–259.
[31] A. Günther, P. Rudolf von Rohr, Large-scale structures in a developed flow over a wavy wall. J. Fluid Mech. 478 (2003) 257–285.
[32] N. Kruse, S. Kuhn, P. Rudolf von Rohr, Wavy wall effects on turbulence production and large-scale modes. J. Turbulence 7 (31) (2006) 1–24.
[33] J.L. Lumley, G.R. Newman, The return to isotropy of homogeneous turbulence. J. Fluid Mech. 82 (1977) 161.
[34] J. Zhou, R.J. Adrian, S. Balachandar, T.M. Kendall, Mechanism for generating coherent packets of hairpin vortices in channel flow. J. Fluid Mech. 387 (1999) 353–396.
[35] R.J. Adrian, K.T. Christensen, Z.-C. Liu, Analysis and interpretation of instantaneous turbulent velocity fields. Exp. Fluids 29 (2000) 275–290.
[36] M.S. Chong, A.E. Perry, B.J. Cantwell, A general classification of three-dimensional flow fields. Phys. Fluids A 2 (5) (1990) 765–777.
[37] K. Hanjalić, S. Kenjereš, Simulation and identification of deterministic structures in thermal and magnetic convection. Ann. N. Y. Acad. Sci. 972 (2002) 19–28.
[38] V. Gnielinski, New equations for heat and mass transfer in turbulent pipe and channel flow. Int. Chem. Eng. 16 (2) (1976) 359–368.
[39] T. Chu, R.J. Goldstein, Turbulent natural convection in a horizontal layer of water. J. Fluid Mech. 60 (1973) 141–159.